TWO APPROACHES FOR REDUCING WASTED 'RED MUD': POSSIBILITY OF UPGRADING BAUXITE AND THE 'RED MUD'

Owada, S[1*], Okajima, D[2], Nakamura, Y[2], Ito, M[3]
[1]Department of Resources and Environmental Engineering, Faculty of Science and Engineering, Waseda University, Japan
[2]Resources and Environmental Science and Engineering, Graduate School of Science and Engineering, Waseda University, Japan
[3]Division of Environment and Resources Engineering, Graduate School of Engineering, Hokkaido University, Japan

Abstract

Red mud is one of the most difficult solid wastes to be reduced and/or recycled from old days in Japan, and many papers have been published for the treatment. However, few commercial plants have operated until now owing to the high cost and low effectiveness of the processing. Our approach can be divided into two categories, one is reducing the amount of red mud by upgrading bauxite and the other one is upgrading the red mud itself for utilization as a raw material of cement and/or iron & steel making industries. To achieve the former objective, we made detail investigation on the existent state of the bauxite ore of Gove mine, Australia, which was imported in Japan at the largest amount. We have found that gibbsite phase, γ-$Al(OH)_3$, in the ore was covered by kaolinite phase, $Al_2Si_2O_5(OH)_4$, and had the possibility to reduce kaolinite content by applying selective surface grinding. To achieve the latter objective, to upgrade the red mud itself, we applied several stages of wet high intensity magnetic separation in a circuit and found the possibility to improve iron content with relatively high recovery. Titanium is one of the major impurities to be reduced from red mud, the existent state (involving mineral species), and the behavior in the circuit of magnetic separation was also clarified.

1 Introduction

The red mud generated from alumina production process has been discharged approx. 700 thousands ton per year in Japan and most of them are disposed in the oceans (Kasai et.al. 1996). Japanese alumina producing companies have been trying to utilize the material from the viewpoint of environmental conservation and effective resources utilization. A lot of research works have been carried out for the red mud, clarifying fundamental mineralogical property (Yanagida, et.al. 1966, Yamada, et.al. 1981, Kasai et.al., 1996, Kinbara, 1993, etc.), treating with sulfur dioxide (Tsai 1971, etc.), nitric acid, reduction & magnetic separation (Colombo, et.al. 1967, etc.), non-reduction sintering & extraction, reduction sintering, melting & extraction, physical separation (Tanjo 1998, Fofana, et.al.1995, etc.), selective flocculation (Das, et.al. 1993, Weissenborn, et.al. 1996, etc.), and the development of modified Bayer process (Harato, et.al., 1996), and so on. Few of the processes, however, have been commercialized because of the difficulties in (1) high cost for drying, (2) removal of sodalite components when utilizing as a raw material in ceramic industry, (3) high recovery of every component because of their low content, and (4) huge amount of the red mud generated.

In this paper, we carried out detailed investigation clarifying the mineralogical property of the original bauxite ore and the red mud, then made a proposal of two kinds of countermeasures, one is upgrading bauxite ore by using selective surface grinding for reducing the amount of red mud generating in the following Bayer process, and the other is applying classification and magnetic separation to the red mud for concentrating iron component.

2 Removal of silicon component from bauxite by surface grinding

2.1 *Sample investigated and the mineralogical property*

Run-of-mine bauxite ore of the Gove mine, Australia was used as a sample. Size distribution is shown in Figure 1, obtained by dry sieving. XRD and XRF analyses were conducted for each size fraction and it was found that major minerals identified in the ore were gibbsite γ-$Al(OH)_3$, hematite Fe_2O_3, kaolinite $Al_2Si_2O_5(OH)_4$, and anatase TiO_2. Figure 2 shows the minerals composition of various size fractions, calculated normatively from the results of XRD and XRF, in which horizontal axis shows the content of each mineral and the width of vertical axis shows the weight ratio of each size range, then, each rectangular area in the figure indicates the weight ratio of each mineral in each size range. The content of kaolinite was found to increase as decreasing particle size and that of gibbsite had a reverse tendency, while the contents of hematite and anatase were kept almost constant with particle size. It must be desirable that the ore processing should be done separately by size ranges, at least in two size ranges, coarser and finer than 1 or 2 mm as a boundary.

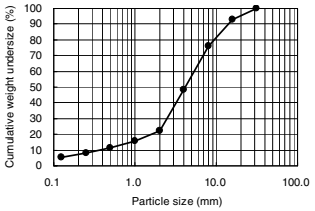

Figure 1: Size distribution of run-of-mine bauxite ore

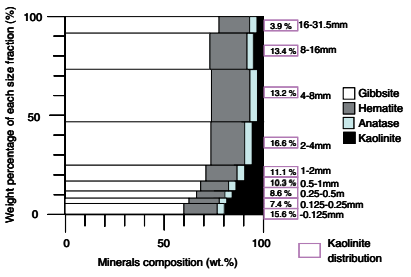

Figure 2: Minerals composition of bauxite ore in various size fractions

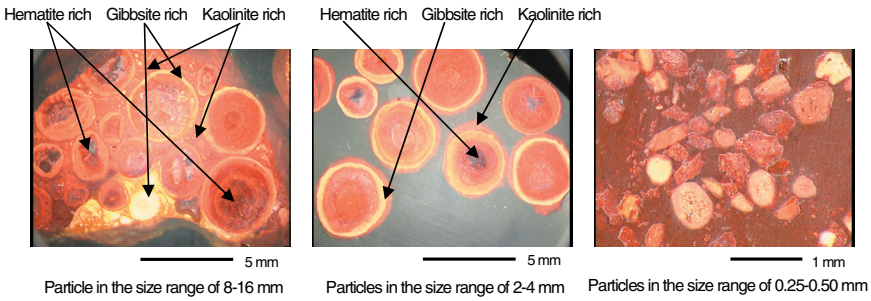

Figure 3: Photomicrographs of typical bauxite particles in different size ranges observed with optical digital microscope

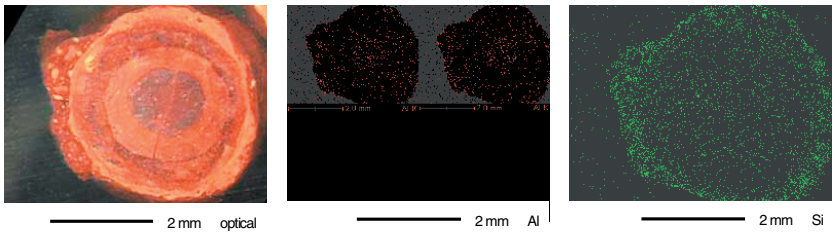

Figure 4: Elemental distribution in a typical bauxite particle obtained with SEM/EDS

Typical photomicrographs observed with optical digital microscope and SEM/EDS are shown in Figures 3 and 4. From many and detailed analyses of the ore, it was identified that gibbsite and hematite rich spherical particles were distributed in the size range of 0.5 to 4.0 mm in the ore, involving outer ring shaped bright area of gibbsite rich phase and inner black area of hematite rich phase, and that kaolinite rich phase was distributed in the area between the spherical particles for the particles of 8–16 mm size range, and the peripheries of spheres for 0.5–4.0 mm size range. In Figure 3, dark grey colored part is rich in hematite, white part is rich in gibbsite and kaolinite, and light grey part of the periphery or outside of spherical particles is rich in kaolinite, and the other light grey part, which is in the spherical particles, shows almost average minerals composition. If we could remove the periphery (light grey color) of spherical particles, in the size range of 0.5 to 4.0 mm, it must facilitate the following processing and lead to the reduction of red mud generation. Micro-Vickers hardness was measured 46 as an average value at the peripheries and 122 inside the spherical particles, then, surface grinding must be reasonable also from this viewpoint.

2.2 *Surface grinding with ball mill*

A laboratory scale alumina ball mill with 120 mm of inner diameter and 100 mm of length was used for the surface grinding in order to reduce kaolinite content. Mill ball size was set at 8 or 20 mm in diameter, and grinding time was set for 15 min or 120 min. Filling rate of the mill ball was set at 20 vol.% of inside mill volume and the ore sample was fed to fill all the open space of the balls. Rotation rate was determined at 49 rpm (39% of critical rate in case using 8 mm ball and 37% in case of 20 mm ball) by using DEM simulator (Inoue, et.al. 1999), for tangential (friction) force, which are ball to ball and ball to wall, to be the maximum and for the normal (compressive) force to be the minimum. As it could be understood in the previous chapter that kaolinite was concentrated at the periphery of spherical particles in the size range of 0.5 to 4.0 mm, we applied the surface grinding to this size range.

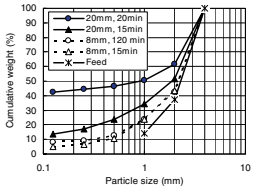

Figure 5: Size distributions of the ground products under various conditions

Size distributions of the ground products under various conditions are shown in Figure 5 and the minerals composition were shown in Figure 6 in the case using 20 mm ball and 15 min of grinding time. From these figures, it is recognized that the finer the size of product is, the higher the kaolinite content becomes in the fractions, in particular, the tendency was obvious in the size range under 0.5 mm. Approx. 44 wt.% of kaolinite can be removed when we obtain only the size range over 0.25 mm as a concentrate. Figure 7 shows the grade and recovery of gibbsite as a function of cut size for compositional separation. Gibbsite grade is almost insensitive to the cut size but the recovery decreases gradually with increasing the cut size. The separation efficiency showed the maximum, 6.4%, at the cut size of 0.25 mm under the conditions of 20 mm mill ball and 15 min grinding time. We can obtain the concentrate of 73.5 wt.% gibbsite content with the recovery of 85% in these conditions.

Considering the size dependency of gibbsite grade in the original bauxite ore (see Figure 2), finer size ranges should be regarded as a tailing, and we can create a processing flowchart of bauxite ore as shown in Figure 8. It has been demonstrated from this flowchart that the concentrate of 74.0 wt.% gibbsite content was separated with gibbsite recovery of 84.3% and kaolinite removal of 35.1%, which indicated that the reduction of the red mud generation was 14.0%.

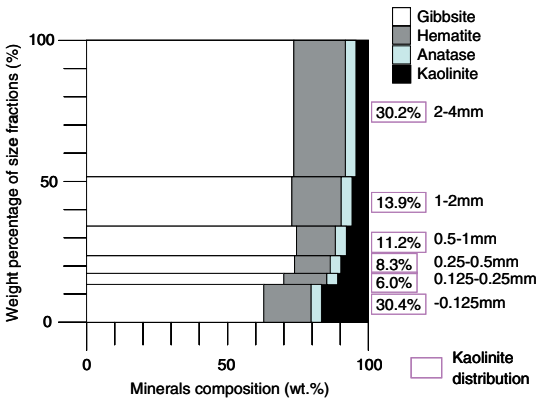

Figure 6: Minerals composition of the ground products in various size fractions under various conditions

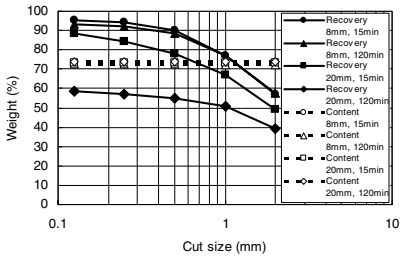

Figure 7: Gibbsite grade and gibbsite recovery as a function of cut size for separation obtained by ball mill grinding with various ball size and grinding time

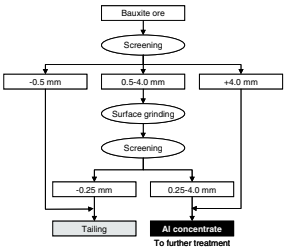

Figure 8: A possible processing flowchart of bauxite ore involving screening and surface grinding

3 Concentration of iron component from red mud by combining cycloning and magnetic separation

3.1 *Sample investigated and the mineralogical property*

The red mud, generated in the Bayer Process treating the Gove ore at Yokohama Plant of the Showa Denko, was used as a sample. The red mud sample was first classified into various size ranges by sieving and elutriation both in 0.2% sodium hexametaphosphate, $(NaPO_3)_6$, water solution, the pH of which was set at 9.0. Elutriation was carried out for the -90μm fractions obtained by sieving and the cut size was set at 2.0 μm. Size distribution of the products (over- and underflow) is shown in Figure 9 and the minerals composition of each size range is shown in Figure 10. Minerals composition was determined by normative calculation from the results of XRD, XRF and SEM/EDS analyses of each size fraction. From Figure 10, we can understand that hematite, Fe_2O_3, and quartz, SiO_2, are concentrated in coarser size ranges, in particular +90 μm and that sodalite group mineral, $Na_6Al_6Si_5O_{22}nH_2O$, gibbsite, γ-$Al(OH)_3$, and anatase, TiO_2, are concentrated in finer size ranges. The size range of +90 μm had 53wt.% of Fe content and 0.84 wt.% of Ti content, then, it would be suitable as a raw material for iron & steel making and/or cement producing industries. For –90 μm size fractions, further treatment should be conducted to increase Fe content and reduce Ti content.

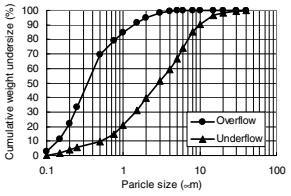

Figure 9: Size distribution of the over-and under-flows obtained by elutriation for –90μm fraction of red mud

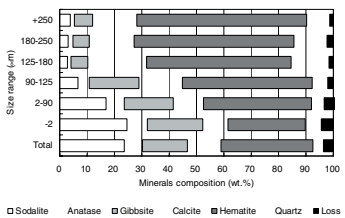

Figure 10: Minerals composition of red mud in various size ranges

3.2 *Classification of –90μm size fraction with cyclone*

In order to utilize the red mud, physical processing methods must be appropriate to apply because of their low energy and cost consumed. Minus several μm or smaller size range is not suitable for the treatment by physical processing, then, it is necessary to classify these slime particles. Krebs cyclone with 0.5 inch diameter and 160 mm length was used for the classification at 3.5 kgf/m^2 of input slurry pressure produced by a Warman pump. Cut size was set at approx. 4–5μm. The –90μm size fraction was divided into cyclone underflow and overflow at the weight ratio of 54 and 46%, respectively.

3.3 *Magnetic separation of cyclone underflow in a single stage*

Iron component in the red mud almost exists in the form of hematite, Fe_2O_3, which reveals para-magnetism at room temperature but with relatively high susceptibility and can be magnetically attractive in strong magnetic fields. We used wet high intensity magnetic separator (WHIMS, Eriez, type L4) with a matrix to recover it, in which the tests were all carried out keeping the separation cell in water sealed to avoid inclusion of air bubbles.

3.4 *Effect of magnetic field*

Three kinds of values of magnetic flux density, 0.8, 1.0, 1.2 T at the separation zone with no matrix, were tested under the conditions, 9–10 of pulp pH and 10 wt.% of pulp density. Iron contents and recoveries of magnetic products were 41, 40, 39 wt.%, and 57, 87, 87%, respectively, in the magnetic flux density of 0.8, 1.0, 1.2 T, and the separation efficiencies were 30, 44, 40%, respectively. Ti contents of magnetic products varied 2.9, 3.2, 3.4 wt.%, which indicated that Ti component also had a considerable magnetization in high magnetic filed and were concentrated in magnetic products.

3.5 *Effect of pulp pH*

Magnetic separation tests were conducted at various pulp pH of 7 to 12, under the conditions of 1.0 T of magnetic flux density and 10 wt.% of pulp density. Optimum pulp pH was determined at 9.0 from the results of Fe & Ti contents, the recoveries to magnetic products, the separation efficiency of hematite from the other minerals, and the dispersion/flocculation behavior of the pulp.

3.6 *Effect of pulp density*

Pulp density is also important to achieve desirable separation, especially, from the viewpoint of dispersion property of the red mud pulp. Here, pulp density was tested at 5 or 10 wt.% which were lower than usual operation condition, for obtaining good dispersion of the pulp. Values of the separation efficiency of hematite from the other minerals were 52 and 45%, respectively for 5 and 10 wt.% of pulp density. In order to achieve good results for concentrating hematite, we adopted 5 wt.% of pulp density in the following tests.

Optimum conditions of magnetic separation could be determined as 5.0 wt.% of pulp density and 9.0 of pulp pH. Under these conditions, the hematite concentrate of 47 wt.% of Fe content was obtained as magnetic product with the recovery of 70%.

3.7 *Magnetic separation of cyclone underflow in a circuit*

Magnetic separation circuit was created as shown in Figure 11 to realize higher Fe content with keeping high recovery. Magnetic flux densities were predetermined at 0.8 to 1.1 T, in order for the Fe content of new feed to be the same as that of feedback flow at each separation in the circuit. Iron contents and the recoveries of the final Fe concentrates in the circuit are shown as filled circles and triangles, respectively, in Figure 12 as a function of circulation time. Here, the experiments were carried out in a manner that no additional new sample was fed to the circuit even in the second and the latter circulation times. Open circles and triangles were Fe contents and the recoveries to the final concentrates, respectively, which were calculated on the assumption that all of the separation results, both of iron distribution into magnetic and non-magnetic products and the separation efficiency, were the same as the results of the magnetic separations in the first circulation. It is found that Fe content and the recovery of the final concentrate are both

converged to the values of 47 wt.% and 83%, respectively, despite slight differences on the way to the final values. From detailed analyses of the final concentrates, size distribution of Fe component was gradually shifted to finer size with increasing circulation time, which confirmed that the larger hematite particles had a tendency to be more attractive in magnetic separation.

Figure 13 shows the simulation results of Fe content and the recovery to the final concentrate, calculated on the same assumption as the above, but that the additional new sample was fed to the top of the circuit so that the quantity of the feed to each circulation was the same as the first feed. It is recognized that both of Fe content and the recovery become almost constant to the values of 50 wt.% and 70%, respectively, after 5 times circulation, which would be the final results when this series of magnetic separation was carried out in a continuous operation.

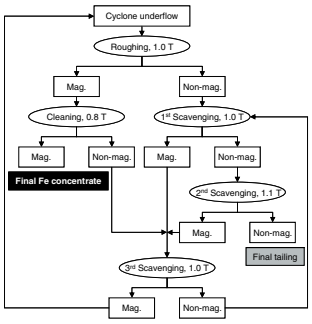

Figure 11: Magnetic separation circuit created for the treatment of cyclone underflow

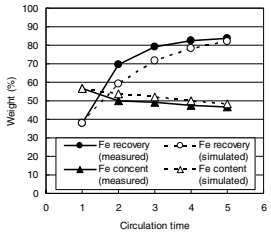

Figure 12: Iron content and Fe Recovery of final product in magnetic separation circuit as a function of circulation time without adding new feed

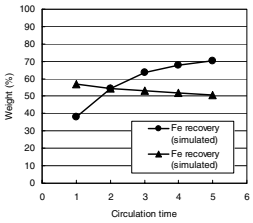

Figure 13: Predicted values of Fe content and Fe recovery of the final product in magnetic separation circuit with adding new sample to the top feed

On the other hand, Ti content of the final product is as much as 3.4 wt.%, which is higher than that of final tailing of 1.0 wt.%. In most of the magnetic separation tests, Ti component had a tendency to be concentrated in magnetic products. Titanium component usually plays a deteriorative role when using it as raw materials both in iron & steel making and cement industries. It was difficult, however, to reduce Ti content of the magnetic products in this paper.

3.8 *Existent state of titanium bearing mineral*

As mentioned above, anatase, TiO_2, was the sole Ti bearing phase identified with XRD, which was known as one of the non-magnetic minerals. Here, we conducted several detailed analyses to clarify the property of Ti bearing minerals with SEM/EDS, and found that these mineral particles consisted both of Ti and Fe components which were distributed almost homogeneously in particles. These kinds of particles, which would be somewhat amorphous, were occupying approx. 70% of all Ti bearing minerals. From the results of simple magnetic separation applied to the non-magnetic products obtained with flux density of 0.4 T, where Ti recovery was found to be only 29%, it was considered that the Ti bearing mineral was not in the form of ilmenite, $FeTiO_3$, and ulvospinel, Fe_2TiO_4, which have relatively strong magnetization. Quantitative analyses were carried out for more than 200 of Ti bearing particles with SEM/EDS and the distribution of the molar ratio, Ti/Fe, was measured (see Figure 14). The most frequent value is situated at around 1.5 of Ti/Fe ratio and the particles have been presumed to be existent as pseudorutile, $Fe_2Ti_3O_9$, like phase (see Figure 15), considering the possibility of generation in the Bayer process. Pseudorutile usually reveals para-magnetism and the susceptibility must be larger than anatase or rutile because of Fe^{3+} ion in the crystal but no stronger than those of ilmenite and ulvospinel, then, it seems difficult to separate them from hematite with magnetic separation.

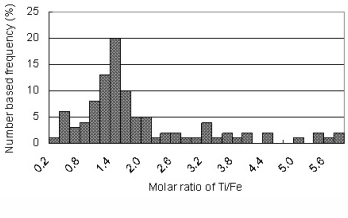

Figure 14: Distribution of Ti/Fe molar ratio of Ti bearing minerals found in non-magnetic products

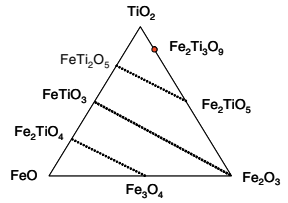

Figure 15 Pseudorutile shown in the triangular diagram of FeO-Fe_3O_4-TiO_2 system.

Figure 15: Pseudorutile shown in the triangular diagram of FeO-Fe_3O_4-TiO_2 system

3.9 *Treatment process of the red mud for concentrating Fe component*

A possible flowchart for processing the red mud can be drawn as shown in Figure 16 to concentrate Fe component. Iron concentrate will be obtained as the +90μm fraction and the final magnetic product of cyclone underflow in the above mentioned magnetic separation circuit, the combined Fe content of which is 51.4 wt.% with the recovery of 57.0%, and the reduction rate of red mud will be reached to 33.3%. However, total Ti content of the combined product is still as much as 2.4 wt.%, then, the amount of utilization must be limited even as a raw material for iron & steel making industry. The rest of the product in the above flowchart will be possible to be transformed such as into zeolite group minerals after the treatment with alkali solution.

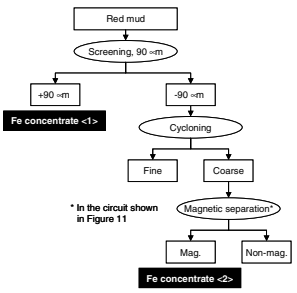

Figure 16: A possible flowchart for processing red mud to concentrate Fe component

4 Conclusion

Two kinds of different approaches were tried in order to reduce red mud generation in the Bayer process, one is selective surface grinding of Gove bauxite ore in a ball mill, and the other is the application of size classification and magnetic separation in a circuit to the red mud itself.

Most of the particles with the size range of 0.5 to 4.0 μm in the Gove bauxite ore were found to be covered with kaolinite rich phase, then, surface grinding was effective in ball mill to this size range, to obtain the Al concentrate of 74.0 wt.% gibbsite content with the gibbsite recovery of 84.3%. In this treatment, with an appropriate size classification, 35% of kaolinite could be removed from this size range, which indicating that the total reduction of red mud generation in the following process was predicted to be 14.0%.

To the red mud of the size range of 4 to 90 μm, magnetic separation was applied creating a new separation circuit, after detailed investigation of the size dependency of minerals composition. It was predicted that the concentrate of 50 wt.% Fe content could be separated with Fe recovery of 70%, by the calculation with a reasonable cycle simulation. However, titanium was also concentrated in the magnetic products. The Ti component was identified as pseudorutile, $Fe_2Ti_3O_9$, like phase which has a considerable magnetic susceptibility in high magnetic field.

A possible flowchart for processing the red mud was designed to concentrate Fe components. From the flowchart, it could be demonstrated that Fe concentrate could be obtained as +90 μm fraction and the magnetic product of cyclone underflow, in which the combined concentrate of 51.4 wt.% Fe content was produced with Fe recovery of 57.0%, and the reduction rate of the red mud could be reached to 33.3%.

References

Colombo, U. and Sironi, B., 1967: 'Process for the production of iron sponge and the recovery of titanium and aluminum from red slurries of bauxite', US Patent, 3295961.

Das, B., Singh, B.P., and Rao, R.B., 1993: 'Recovery of iron values from red mud by selective flocculation', Indian Chemical Engineering, vol.35, no.3, pp. 154–156.

Fofana, M., Kmet, S., Kunhalmi, G., Jakabsky, S., and Hredza, K.S., 1995: 'Treatment of red mud from alumina production by high-intensity magnetic separation', Magnetic and Electrostatic Separation, vol.6, no.4, pp. 243–251.

Harato, T., Ishida, T., Kato, H., Inami, M., Ishibashi, K., Kumagae, Y., and Murakami, M., 1996: 'The development of a new Bayer process that reduces the desilication loss of soda by 50% compared to conventional process', 4th Aluminum Quality Workshop, Darwin, June, pp. 312–320.

Inoue, T., Okaya, K., Owada, S., and Homma, T., 1999: 'Development of a centrifugal mill – a chain of simulation, equipment design and model validation', Powder Technology, vol.105, no.1, pp. 342–350.

Kasai, H. and Saito, F., 1996: 'Resource recovery of bauxite residue in the ceramic material manufacturing', Metals & Technology, Temporary number, pp. 105–114.

Kasai, T and Mizota, T, 1996: 'Utilization of red mud exhausted from alumina production industry', Journal of Mining and Materials Processing Institute of Japan, vol.112, no.3, pp. 131–139.

Kinbara, M., 1993: 'Problem of resources and recycling 2. Red mud and its utilization', Kougyo to Seihin, no.58, pp. 42–46.

Tanjo, M.: 'Material processing with the aim of recycling society. Technology development for treatment of red mud. Bauxite enrichment and effective utilization to raw material for iron making', Kinzoku, vol.68, no.9, pp. 785–793.

Tsai, J.H., 1971: Process for the separation of useful compounds from waste of the aluminum industry, US Patent, 3574537.

Weissenborn, P.K., Warren, L.J., and Dunn, J.G., 1996: 'Behavior of amylopectin and amylose components of starch in the selective flocculation of ultrafine iron ore', International Journal of Mineral Processing, voll.47, no.3, pp. 197–211.

Yanagida, U. and Yamaguchi, G., 1966: 'A discussion on the phase diagram of the system Al_2O_3-H_2O considering the transformation mechanism of the polymorphs appearing it', Journal of Ceramic Society of Japan, vol.74, no.3, pp. 94–100.

Yamada, K., Harato, T. and Shiozaki, H., 1981: 'Flocculation and sedimentation of red mud', Journal of Japan Institute of Light Metals, vol.31, no.1, pp. 37–42.